Thermoelectric properties of pressure-sintered $Si_{0.8}Ge_{0.2}$ thermoelectric alloys

Cronin B. Vining
Jet Propulsion Laboratory, California Institute of Technology, 4800 Oak Grove Drive, Pasadena, California 91109

William Laskow, Jack O. Hanson, Roland R. Van der Beck, and Paul D. Gorsuch
General Electric Company, P. O. Box 8555, Philadelphia, Pennsylvania 19101

(Received 2 March 1990; accepted for publication 29 November 1990)

The thermoelectric properties of 28 sintered $Si_{0.8}$ $Ge_{0.2}$ alloys, heavily doped with either boron or phosphorus and prepared from powders with median particle sizes ranging from about 1 μm to over 100 μm, have been determined from 300 to 1300 K. The thermal conductivity decreases with decreasing particle size, however, the figure of merit is not significantly increased due to a compensating reduction in the electrical conductivity. The thermoelectric figure of merit is in good agreement with results of Dismukes *et al.* [J. Appl. Phys. **10**, 2899 (1964)] on similarly doped alloys prepared by zone-leveling techniques. The electrical and thermal conductivity are found to be sensitive to preparation procedure while the Seebeck coefficient and figure of merit are much less sensitive. The high-temperature electrical properties are consistent with charge carrier scattering by acoustic or optical phonons.

I. INTRODUCTION

The thermoelectric properties of large-grain silicon-germanium alloys have been examined by Dismukes *et al.*[1] using high- quality, zone-leveled materials. This report examines the hypothesis of Rowe and others[2–5] that sintered silicon-germanium alloys may be superior to single-crystal materials for use in thermoelectric energy conversion applications. Apart from practical advantages such as ease of preparation and superior mechanical strength afforded by the use of sintered materials, previous theoretical[2,6–12] and experimental[2–4,13,14] evidence had suggested that phonon scattering at grain boundaries reduces the thermal conductivity, k, compared to single-crystal alloys of the same composition. Since the conversion efficiency of a thermoelectric heat engine depends on the temperature range of operation and material properties through the dimensionless figure of merit $ZT = S^2\sigma T/k$, where S is the Seebeck coefficient, σ is the electrical conductivity, and T is the temperature, a reduction in k should result in an increased figure of merit, and therefore conversion efficiency, if the other properties remain unchanged. This effort reflected results of recent reviews on thermoelectricity in general[15] and heavily doped silicon germanium in particular.[5]

Goldsmid and Penn[6] first pointed out that boundary scattering may significantly reduce the thermal conductivity in solid solutions, even for characteristic boundary scattering length scales much larger than a typical phonon mean free path, because a relatively large proportion of the heat is carried by long wavelength phonons. Further theoretical calculations based the Klemens–Callaway formalism[16,17] have allowed estimates of the magnitude of the reduction in k for undoped[6,7] and heavily doped[2,8–12] silicon germanium of as large as 50% for particle sizes of 1 μm. As carrier mean- free-path lengths are much smaller than 1 μm, several authors have suggested pressure- sintered materials might exhibit electrical properties essentially identical to single- crystal materials[2,8,12,14] with proper preparation. Some reports of electrical resistivity measurements[2,18–21] on sintered materials support this view in the best cases, but more often the electrical resistivity of the sintered materials are higher than zone leveled materials.[1] In no case had the anticipated improvement in figure of merit due to grain-boundary scattering been realized experimentally in silicon- germanium alloys, with the possible exception of one report in which GaP was combined with silicon germanium.[2]

This paper summarizes experimental results which confirm the reported reduction of the thermal conductivity of sintered materials compared to similar zone-leveled materials. It is accompanied, however, by a highly correlated, compensating degradation in the electrical properties. Thus, there is no overall improvement in the figure of merit with reduction in grain size. The temperature dependence of the observed reduction in the thermal conductivity appears to be inconsistent with the Klemens–Callaway formalism calculations, suggesting that the reduction in thermal conductivity may be due to an altogether different mechanism, one which affects the electrical conductivity in a similar manner.

II. EXPERIMENTAL DETAILS

Fifty five (55) compacts of silicon germanium alloys were prepared by vacuum hot pressing of powders made by a variety of techniques. The starting point for 50 of these compacts was the induction melting of silicon and germanium in a 4-to-1 atomic ratio in fused silica crucibles under high vacuum. n-type materials were prepared by adding 0.55 wt % phosphorus to the melt while p-type samples were prepared with 0.08 wt. % boron in the crucible. Some exceptions are indicated in Table I. The melt was cast into

 0021-8979/91/084333-08$03.00

TABLE I. Summary of preparation method and properties of $Si_{0.8}Ge_{0.2}$. Soak time = 30 min and soak temperature = 1513 K, unless noted.

Sample preparation		esd[u] (μm)	k (W/m k)	S (μV/K)	σ (Ω m) 10^{-5}	μ (m^2/Vs) 10^{-4}	n (m^{-3}) 10^{26}	Density (g/m^{-3}) 10^7	ZT maximum	Oxygen[v] (wt. %)
n-type samples: phosphorus content = 0.59a/o (unless otherwise noted)										
3332	a	>174	4.66	−108.9	0.87	55.8	1.29	3.05	0.917	0.14
68	a	124	5.03	−121.6	1.06	55.1	1.07	2.87	0.832	0.17
110	b	15.0	4.51	−97.7	0.73	51.1	1.68	3.01	0.972	
111	b	16.0	4.47	−102.3	0.78	51.9	1.54	2.99		
69	a	13.5	4.82	−116.4	0.93	52.7	1.28	3.04	0.762	0.24
130	a,c	5.0	5.09	−104.2	0.85	53.2	1.39	2.92	0.942	
70	a,d	3.9	4.17	−114.3	1.07	46.4	1.26	3.02	0.967	0.91
79	a,c	2.4	3.81	−119.5	1.30	41.4	1.16	2.98		
63	a,c	3.3	4.11	−112.3	1.09	44.8	1.28	2.99	0.969	1.00
81	a,e	3.3	3.54	−121.4	1.30	43.0	1.12	3.01	0.971	1.31
116	a,f	2.8	4.43	−119.2	0.98	53.7	1.19	2.94		
93	a,c,j	1.8	3.97	−115.9	1.15	43.8	1.25	2.96	1.040	0.92
84	a,g	1.3	3.74	−117.2	1.14	46.5	1.18	2.96	0.952	2.93
152	c,k	2.1	3.81	−110.8	1.03	47.2	1.29	3.02	0.943	
151	c,l	2.4	3.83	−110.6	1.04	46.3	1.30	2.99	0.918	
153	c,m	1.9	3.90	−105.0	0.91	49.4	1.39	3.01	0.920	
p-type samples: boron content = 0.23 a/o (unless otherwise noted)										
3334	a	>174	5.00	112.5	1.07	34.2	1.72	3.01	0.522	0.21
73	a	124	5.02	114.6	1.16	32.5	1.66	2.87	0.568	0.15
112	b	15.0	4.96	117.8	1.07	33.7	1.73	2.98		
74	a	11.0	5.25	117.0	1.14	32.8	1.67	2.94	0.501	0.28
131	a,c	6.1	4.75	117.7	1.11	34.2	1.64	2.99	0.506	
78	a	4.5	4.37	119.5	1.28	31.5	1.55	2.98	0.619	0.99
62	a,c	4.1	4.26	124.2	1.34	31.1	1.50	2.99	0.564	1.00
72	a,e	3.0	3.32	131.3	2.06	25.1	1.21	2.98	0.537	2.20
117	a,f	2.8	4.86	123.5	1.25	34.6	1.46	2.96		
99	a,h	2.7	3.99	133.5	1.68	29.8	1.25	2.99		1.49
75	a	2.6	3.88	120.9	1.39	29.2	1.54	2.96	0.619	1.53
60	a,c	2.3	4.30	123.3	1.36	31.1	1.48	3.00		
82	a,e	2.3	3.22	132.3	1.78	27.9	1.26	2.97	0.564	1.73
103	a,c	2.2	3.93	131.4	1.86	29.7	1.13	3.00		0.91
104	a,c,n	2.2	3.24	133.4	2.24	26.8	1.04	3.00		4.68
101	a,h	1.6	4.10	131.7	1.62	31.3	1.23	3.02		0.37
102	a,h,o	1.5	3.90	139.0	2.11	30.2	0.98	3.03	0.519	0.23
83	a,g	1.3	3.63	124.2	1.70	27.6	1.33	2.95	0.535	2.84
124	a,p	8.1	5.73	278.4				2.98	0.184	
11	a,q	>44	5.32	79.2	0.55	33.2	3.45	3.00		
12	a,r	>44	5.31	80.2	0.55	33.2	3.45	3.00		
13	a,s	>44	5.44	78.8	0.54	32.1	3.61	2.99		
14	a,t	>44	5.42	80.2				2.98		
66	i	4.2	4.18	149.5	2.39	29.3	0.89	2.97		
66A	i	4.6	3.77	150.6	2.65	28.7	0.82	2.96	0.523	
Vary sintering soak time										
86	15 min	2.0	3.62	127.4	1.67	28.4	1.32	2.93		1.52
88	30 min	2.0	3.78	127.5	1.63	28.2	1.36	2.96		
87	60 min	2.0	4.03	127.1	1.50	29.1	1.43	2.98		
The following four samples were prepared from a single lot of powder[a,c]										
Vary sintering soak temperature, Series A										
89	1513 K	2.2	3.68	129.6	1.69	27.0	1.37	2.94		
90	1528 K	2.2	3.91	126.5	1.54	29.3	1.38	2.96		
91	1543 K	2.2	4.05	124.2	1.40	30.9	1.44	2.99		
92	1558 K	2.2	4.49	124.7	1.39	30.8	1.46	3.00		1.50

TABLE I. (*continued*).

Sample preparation		esd[u] (μm)	k (W/m k)	S (μV/K)	σ (Ω m) 10^{-5}	μ (m^2/Vs) 10^{-4}	n (m^{-3}) 10^{26}	Density (g/m^{-3}) 10^7	ZT maximum	Oxygen[v] (wt. %)
The following four samples were prepared from a single lot of powder[a,c]										
Vary sintering soak temperature, Series B										
97	1513 K	1.9	3.90	129.7	1.31	32.6	1.46	2.98	0.565	1.60
94	1573 K	1.9	4.18	122.7	1.30	33.0	1.45	3.00		
95	1588 K	1.9	4.35	123.4	1.20	31.9	1.64	2.96		
96	1603 K	1.9	4.54	123.1	1.22	28.2	1.82	2.94		
The following three samples were not intentionally doped										
2		124	7.03					2.88		
8		16	6.65		2240			3.00		
1	a,f	2.5	3.75					2.88		

[a]Pulverization in a shatter box.
[b]Gas atomization from the melt (Ref. 23).
[c]Planetary ball milling in agate using agate balls in a hydrocarbon.
[d]Planetary ball milling in agate using dry agate balls.
[e]Attrition milled (Ref. 24).
[f]Air jet pulverization.
[g]Planetary ball milling in agate using agate balls in water.
[h]Planetary ball milling in steel using steel balls in a hydrocarbon.
[i]Hot-pressed mixture of elemental silicon, germanium, and boron.
[j]Limited exposure of the powder to air before sintering.
[k]0.77 at. % phosphorus.
[l]0.9 at. % phosphorus.
[m]2.0 at. % phosphorus.
[n]Same powder lot as 103, but roasted in air at 773 K before sintering.
[o]Powder was handled under an inert atmosphere through sintering.
[p]0.025 at. % boron.
[q]1.0 at. % boron.
[r]2.0 at. % boron.
[s]4.0 at. % boron.
[t]8.0 at. % boron.
[u]Equivalent spherical diameter.
[v]Oxygen content determined by neutron activation analysis.

a water-cooled copper to produce a 400-g ingot which was mechanically pulverized to -80 mesh powder. The resulting powders were then subjected to a variety of different comminution techniques in order to achieve various median particle sizes. Table I summarizes the comminution techniques employed and the particle sizes achieved.

Three compacts were prepared from alloy powders produced by a gas atomization technique,[23] and two compacts were prepared by direct sintering of mixed powders of elemental silicon, germanium and boron.

The particle sizes listed in Table I were determined on the powders with a Micromeritics Sedigraph 5000D. The particle sizes were also determined by optical metallography on most of the hot-pressed compacts. A good correlation was observed between the particle sizes determined by the two techniques. However, the microstructure of these alloys may be somewhat more complex as Owusu-Sekyere *et al.* have shown[25] that grains smaller than those revealed by either the Micromeritics or optical methods can be seen in transmission electron microscopy tests.

Pressure sintering was performed in a double- action vacuum hot press with a vacuum level of about 8×10^{-5} Torr. TZM dies and molds with a light graphite coating to reduce friction during compact ejection were used. The pressing pressure was 180 MPa of pressure, applied after achieving the soak temperatures. The heating rate to the soak temperature was about 25 K/min. After soaking at temperature (see Table I for soak times and temperatures), pressure was released and the compact ejected from the die. Furnace power was then turned off and the furnace allowed to cool. The resulting compacts were 5.08 cm diameter by 1.27 cm thick, dense, crack- free, and dull gray in appearance.

The compact surfaces were machined flat and parallel and the thermal conductivity of the compact was measured at 370 K by a standardized steady-state technique (ASTM designation F-433) calibrated by measurements on Pyroceram 9806 and Pyrex 7740 with about a 10- K temperature drop across the compact. The precision of these measurements were better than $\pm1\%$ and the accuracy is believed to be better than $\pm5\%$. The Seebeck coefficient was determined at room temperature as the ratio of the voltage developed between two Cu probes in contact with the sample, one probe about 15 K warmer than the other, and the temperature difference between the Cu probes as measured by thermocouples placed very near the points of contact of the probes with the sample. Density was determined using an immersion technique. The electrical resistivity and Hall coefficient, from which the carrier concentration and Hall mobility were calculated, were determined using van der Pauw's technique[26] on 1.27- cm-diam, 0.08-cm-thick samples cut from each compact. Neutron activation analysis for oxygen content was performed on 25 samples.

High-temperature measurements of thermal diffusivity, Seebeck coefficient, and electrical resistivity were performed on 14 n-type and 14 p-type compacts. The thermal diffusivity was determined using a standard laser flash technique[27] between 400 and 1380 K in 100-K increments, generally on the same sample used in the Hall measurements. Repeated measurements on a single sample indicate a reproducibility of better than $\pm3\%$ over the entire tem-

perature range. The high-temperature thermal conductivity was calculated using the measured density, corrected for thermal expansion, and heat capacity results determined by a drop calorimetry technique.[28] A single set of heat capacity data was used for all thermal conductivity calculations.

High-temperature electrical resistivity and Seebeck measurements were performed simultaneously on a 0.63 cm × 0.63 cm × 4.6 cm sample cut from each compact and instrumented with four chromel-alumel thermocouples cemented in equally spaced holes with a graphite cement. To prevent reaction with the sample each thermocouple was coated with a thin layer of graphite cement before mounting in the sample. The sample was placed in a vacuum furnace between independently controlled resistance heaters. The Seebeck coefficient was determined from the slope of the voltages measured between the thermocouple legs plotted against the temperature differences between the thermocouples. The temperature difference across the sample was typically 10–30 K during this measurement.

The Seebeck coefficient data were corrected for the absolute Seebeck coefficient of the leads as determined in an independent measurement of the absolute Seebeck coefficients of chromel and alumel with respect to platinum, incorporating literature values for the absolute Seebeck coefficient of platinum.[29] The corrections for absolute are believed accurate to within ±2 μV/K. The precision and reproducibility of the Seebeck coefficient measurements was better than 1%, as determined on relatively stable *p*-type silicon-germanium samples. While more difficult to estimate since no standard materials with large Seebeck coefficients are available, the accuracy of these measurements are believed to be comparable to the precision.

The electrical resistance was measured using an ESI 1700 resistance bridge with 1-μΩ resolution employing a low-frequency square-wave, four-probe technique with the sample supports serving as current leads. The resistivity was calculated as the slope of six independent resistance measurements determined along the length of the sample plotted against the distances between the thermocouples, multiplied by the cross-sectional area of the sample. The principal source of error in the resistivity determination was dimensional uncertainty. The precision of the resistivity measurements was better than ±0.5% with similar accuracy. Approximately 100 Seebeck coefficient and electrical resistivity data points were collected between about 300 and 1300 K by an automated data collection and data reduction system.

III. EXPERIMENTAL RESULTS

Table I summarizes the results of room-temperature measurements of the median particle size of the feed powder, thermal conductivity, Seebeck coefficient, electrical resistivity, Hall mobility, carrier concentration, density and oxygen content for each of the alloys, as well as the hot-pressing conditions used. The maximum ZT values calculated from the high-temperature thermoelectric property measurements on 26 of the alloys are also summarized. As an aid in analyzing the results of Table I, previous room temperature results[1] on zone-leveled $Si_{0.8}$ $Ge_{0.2}$ have been parametrized using a purely empirical interpolation scheme as follows:

p — type:

$$\ln(S_{zl}) = -0.451 \ln(n) + 5.02,$$

$$\ln(\mu_{zl}) = -0.116 \ln(n) + 3.75,$$

$$\ln(k_{zl}) = -0.089 \ln(n) + 1.78,$$

n — type:

$$\ln(-S_{zl}) = -0.502 \ln(n) + 4.82,$$

$$\ln(\mu_{zl}) = -0.300 \ln(n) + 4.19,$$

$$\ln(k_{zl}) = -0.085 \ln(n) + 1.67,$$

with S_{zl} in μV/K, μ_{zl} in 10^{-4} m^2/V s, k_{zl} in W/m K, and n in 10^{26} m^{-3}. The measured thermal conductivity of a sintered sample has been normalized by calculating the thermal conductivity of a corresponding zone- leveled sample using the Hall carrier concentration of the sintered sample and the zone-leveled data above. The resulting ratio of measured to calculated thermal conductivities is shown as a function of the feed particle size in Fig. 1 for 20 *p*-type samples of sintered $Si_{0.8}Ge_{0.2}$. Samples prepared using similar comminution techniques and sintered under similar conditions (compact Nos. 62, 74, 75, 78, 83, 99, 131, indicated by the open circles) show a systematic decrease in thermal conductivity as the particle size decreases.

For constant particle size, the thermal conductivity increases systematically with increasing sintering time (indicated by TIME: compact Nos. 86, 87, and 88) or increasing sintering temperature (TEMPERATURE: compact Nos. 89, 90, 91, and 92), as indicated by the two sets of data connected by vertical lines in Fig. 1. Variations in preparation technique also significantly affect the thermal conductivity as indicated by the samples produced by gas atomization (GA: compact No. 112) and alternate comminution techniques such as air jet pulverization (AJP:

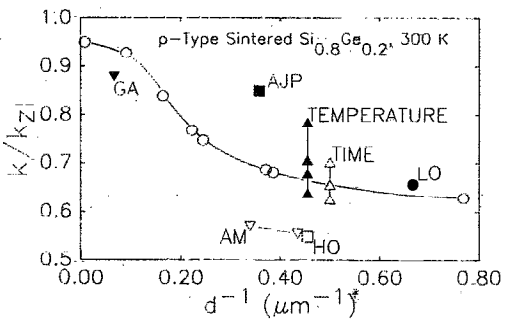

FIG. 1. The thermal conductivity of sintered heavily doped *p*-type $Si_{0.8}Ge_{0.2}$, normalized to the thermal conductivity of zone-leveled material with the same carrier concentration, as a function of feed particle size. The data labeled TEMPERATURE and TIME indicate the effect of hot-pressing temperature and soak time, respectively, while the data labeled GA, AJP, AM, HO, and LO indicate the effect of variations in the powder comminution process.

compact No. 117) and attrition milling (AM: compact no. 72 and 82). Intentionally increasing the oxygen content (HO: compact No. 104) by roasting the powder in air resulted in a significant further reduction in the thermal conductivity, while a decrease in the oxygen content produced by handling the powder exclusively under an inert atmosphere (LO: compact No. 102) may have resulted in a slight increase.

A normalization procedure similar to that described above for the thermal conductivity results had been also been applied to the Hall mobility resuIts. Figure 2 shows the Hall mobility values, normalized to the Hall mobility of zone-leveled[1] alloys of the same carrier concentration, obtained on the same 20 samples described above. The behavior of the mobility is seen to be qualitatively similar to the thermal conductivity, with a few exceptions, and a strong correlation between thermal conductivity and Hall mobility is observed.

To demonstrate this effect the quantity $S^2\sigma$, sometimes called the electrical power factor, has been normalized to similarly doped zone- leveled material in the same way as described above for the thermal conductivity. Since the Seebeck coefficient is expected to be a function of the carrier concentration alone, the normalized power factor is expected to be identical to the normalized Hall mobility. Figure 3 shows the normalized electrical power factor plotted against the normalized thermal conductivity for the samples listed in Table I. The point (1,1) in Fig. 3, indicated by the end of the solid line, represents zone- leveled material and the solid line connects the origin with this point. A data point above this line represents a figure of merit higher than zone- leveled material and a point below this line represents a lower figure of merit compared to zone leveled material. While there is considerable scatter in the data shown in Fig. 3, the general correlation between electrical and thermal properties is quite strong. Since the thermal conductivity data in Fig. 1 is determined on the full 5.08-cm compacts, while the electrical mobility and electrical conductivity in Figs. 2 and 3 are determined on a thin sample cut from the compact, some of the scatter in Fig. 3 may be attributed to inhomogeneities within the compacts.

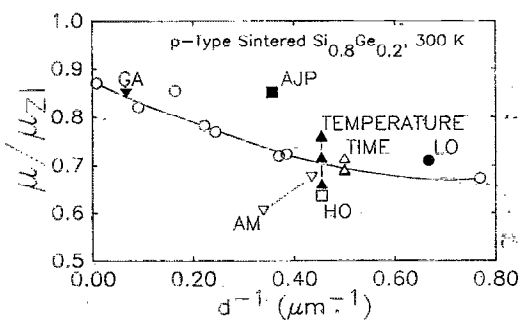

FIG. 2. Hall mobility of sintered, heavily doped, p-type $Si_{0.8}Ge_{0.2}$, normalized to the Hall mobility of zone-leveled material with the same carrier concentration, as a function of feed particle size. The data labeled TEMPERATURE and TIME indicate the effect of hot pressing temperature and soak time, respectively, while the data labeled GA, AJP, AM, HO and LO indicate the effect of variations in the powder comminution process.

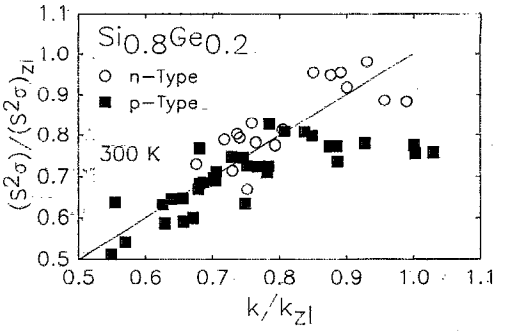

FIG. 3. Electrical power factor as a function of thermal conductivity of sintered $Si_{0.8}Ge_{0.2}$ normalized to the electrical power factor of zone-leveled material with the same carrier concentration. The solid line represents a figure of merit equivalent to zone-leveled material.

Figure 4 shows the Seebeck coefficient, electrical resistivity, thermal conductivity, and figure of merit for sintered n-type (93) and p-type (75) samples from this study and sample 1834 from Dismukes,[1] the only zone-leveled $Si_{0.8}Ge_{0.2}$ sample characterized at high temperatures in that

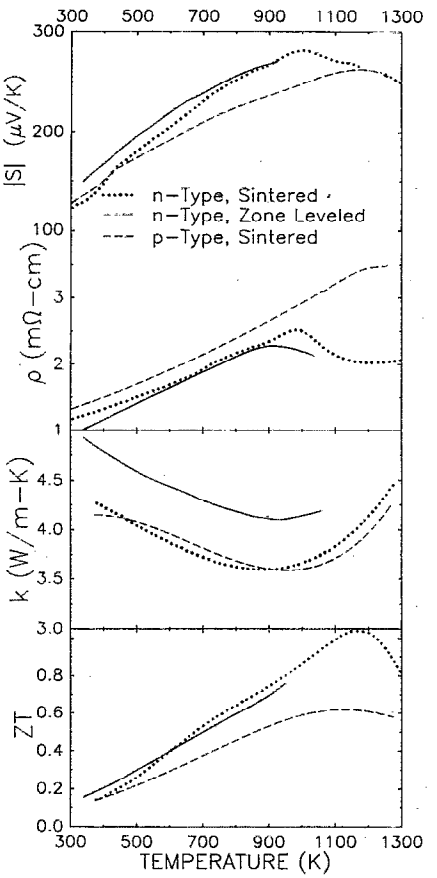

FIG. 4. Seebeck coefficient, electrical resistivity, thermal conductivity, and figure of merit as a function of temperature for n and p-type sintered $Si_{0.8}Ge_{0.2}$ and n-type zone-leveled $Si_{0.8}Ge_{0.2}$ (see Ref. 1).

study. The agreement between the figure of merit of the sintered and zone- leveled materials is quite good and probably within experimental error. While the data in Fig. 4 are typical of the quality of the high- temperature data collected, the two samples selected as examples represent the highest figure of merit observed in this study.

The thermal conductivity of five samples (compact Nos. 73, 74, 83, 62, and 72) of p-type sintered $Si_{0.8}Ge_{0.2}$ at elevated temperatures, normalized to the thermal conductivity of the largest particle size sample (73) is shown in Fig. 5. The thermal conductivity generally decreases with decreasing particle size, with the exception of sample 72 (3.0 μm), which was prepared by attrition milling, consistent with the low-temperature, steady-state thermal conductivity data shown in Fig. 1. The normalized conductivity appears to be nearly independent of temperature between 300 and about 1000 K. Above 1000 K the conductivity of the smaller particle size samples approaches the conductivity of the larger particle size samples.

Figure 6 shows a combined plot of the Seebeck coefficient and the electrical conductivity. Following Jonker[30] a S-σ plot can be described by:

$$S=\pm\frac{k}{2e}\left(\frac{E_g}{kT}+A_+ +A_-\right)\left(1-\frac{\sigma_{\min}}{\sigma^2}\right)^{1/2} -\frac{k}{e}\ln\left\{\frac{\sigma}{\sigma_{\min}}\left[1\pm\left(1-\frac{\sigma_{\min}}{\sigma^2}\right)^{1/2}\right]\right\} +\frac{k}{2e}\ln\left(\frac{N_- e^{A+}\mu_-}{N_+ e^{A-}\mu_+}\right), \quad (1)$$

where $N_\pm$, $\mu_\pm$ and $A_\pm$ are the density of states, mobilities, and transport coefficients, respectively, of holes (+) and electrons (−). The solid line in Fig. 6 represents a fit of the data at 1200 K to Eq. (1) with

$$(E_g/k_BT+A_+ +A_-)=11.01\pm0.08,$$

$$\sigma_{\min}=6170\pm40\ \Omega^{-1}m^{-1},$$

and

$$N_+e^{A+}\mu_+/N_-e^{A-}\mu_-=0.59\pm0.05.$$

Much of the scatter in Fig. 6 is attributed to variations

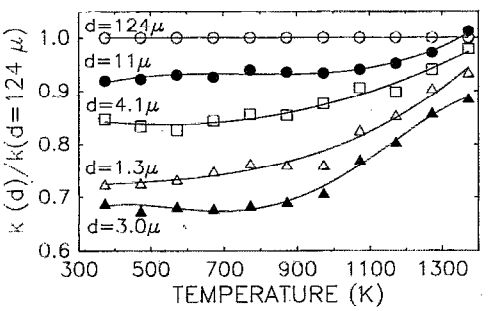

FIG. 5. Thermal conductivity of five samples of sintered, p-type $Si_{0.8}Ge_{0.2}$ (73, 74, 83, 62, and 72), normalized to the thermal conductivity of the largest particle size sample (73), as a function of temperature.

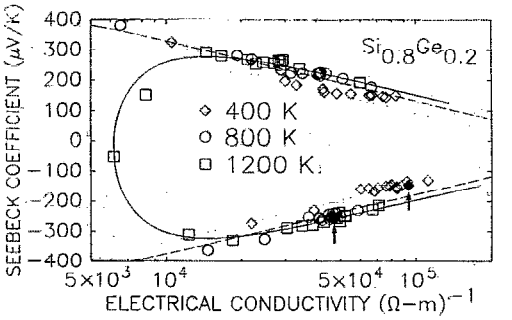

FIG. 6. The Seebeck coefficient of $Si_{0.8}Ge_{0.2}$ as a function of electrical conductivity. The solid line is a theoretical fit to the data at 1200 K. The dashed and dotted lines indicate a theoretical extrapolation to 800 and 400 K, respectively, based upon the fit at 1200 K. The arrows and solid circles indicate previous data on zone-leveled material (see Ref. 1).

in electrical mobility resulting from the sintering processing. The systematic variations in electrical properties, which correlate with the thermal conductivity (Figure 1) and not with carrier concentration, are too small in magnitude to mask the much larger doping effects and hence appear as scatter in Fig. 6. The dashed and dotted lines in Fig. 6 represent calculated Seebeck coefficient at 800 and 400K, respectively, based upon Eq. (1), the coefficients resulting from the fit to the data at 1200 K and taking into account the temperature variation of $\sigma_{\min}$, but with no additional adjustable parameters. The agreement between the experimental data and the theoretical curves is quite reasonable, although the p-type data at 400 K deviate somewhat from the predicted curve based upon the 1200-K data. The curvature of the p-type data at 400 K may be indicative of degenerate statistics and the close agreement between the data and the calculated curves at 800 and 1200 K indicate degeneracy of the carriers has been lifted by 800 K.

Literature estimates of the temperature variation of the energy gap of Si vary from $dE_g/dT=2.3$ (Ref. 31) to 4.3×10^{-4} eV/K.[32] Using E_g (0 K) = 1.07 eV and assuming the same scattering mechanism for electrons and holes gives $A_-=A_+=1.7$ to 2.8, indicating either acoustic ($A=2$) or optical ($A=3$) phonon scattering of carriers as the dominant scattering mechanism. Insufficient data are available in the low-conductivity region of Fig. 6 to allow a more definitive, independent estimate of dE_g/dT, and hence the scattering mechanism remains somewhat uncertain.

Figures 7 and 8 show the electrical power factor ($S^2\sigma T$), in thermal conductivity units, as a function of thermal conductivity for n-type and p-type $Si_{0.8}Ge_{0.2}$, respectively. The correlation of electrical and thermal properties shown in Fig. 3 at room temperature is also evident in the high-temperature data, although somewhat less clearly due to carrier concentration variations. The electrical and thermal properties of sintered n-type $Si_{0.8}Ge_{0.2}$ shown in Figs. 6 and 7 can be as good as the results of Dismukes[1] on zone- leveled material of the same composition; however, many samples exhibit lower k and lower $S^2\sigma T$ values.

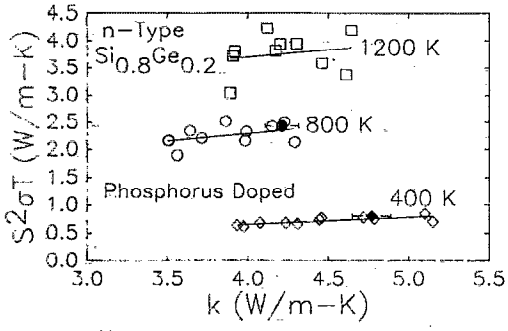

FIG. 7. Correlation between electrical power factor ($S^2\sigma T$) and thermal conductivity in sintered n-type $Si_{0.8}Ge_{0.2}$. Error bars indicate $\pm 2.5\%$ and are not actual estimates of the error. Solid lines are least-square fits to the data.

IV. DISCUSSION

While the reduction in the thermal conductivity due to reduced particle size (Fig. 1) has been ascribed to grain-boundary scattering of phonons, the correlation between both the Hall mobility and electrical power factor and the thermal conductivity, indicated by the normalized room-temperature results shown in Figs. 2 and 3 and supported by the high-temperature results of Figs. 7 and 8, is somewhat surprising. Numerous authors have discussed the effect of grain-boundary scattering on thermal conductivity,[2-13] but the effect on the electrical conductivity of heavily doped silicon germanium is often neglected because the electron mean free path is estimated to be several orders of magnitude smaller than the expected grain-boundary scattering length.

In polycrystalline Si, however, significant reduction in carrier mobility, due to potential scattering at grain boundaries, is well documented, and can amount to several orders of magnitude at low doping levels.[33] While discussing 0.2-μm grain size, heavily doped ($\geqslant 10^{25}$ carriers/m^3) polycrystalline Si Seager comments that "the mobility will approach (within, say factors of 2 or 3) single-crystal values" (see Ref. 33, p. 296). As sintered materials can be expected to have more disordered grain boundaries than typical of polycrystalline Si, mobility reductions on the order of 10%–50% seem quite plausible for 1-μm particle size sintered materials due to grain-boundary effects alone.

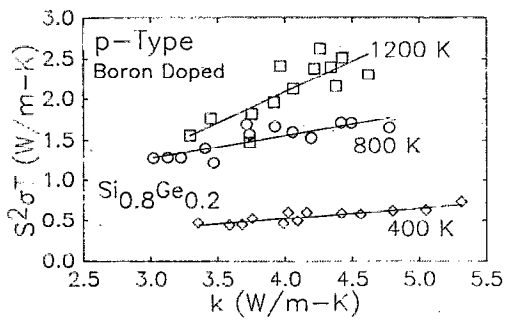

FIG. 8. Correlation between electrical power factor ($S^2\sigma T$) and thermal conductivity in sintered p-type $Si_{0.8}Ge_{0.2}$. Solid lines are least-square fits to the data.

The highly correlated reduction in the electrical and thermal properties observed here may be the result of these two physically different scattering mechanisms for carriers and phonons, both of which may happen to be about the same order of magnitude and correlate well with particle size. The different nature of the scattering mechanisms, however, suggests rather different temperature dependencies would be expected. While there is considerable scatter in the data, Figs. 6 and 7 suggest the correlation observed at room temperature in Fig. 3 persists in approximately the same form at high temperature.

Perhaps more significant is the temperature independence of the reduction in the thermal conductivity due to particle size effects up to about 1000 K and the pronounced change in the temperature dependence at about 1000 K (Fig. 4). All of the contributions to the thermal conductivity are presumably similar for the samples shown, with the exception of sintering-related effects. As the average phonon mean free path decreases with increasing temperature, the effect of grain boundaries is expected to become less important with increasing temperature. Neither the observed temperature independence below 1000 K nor the more rapid temperature dependence above this temperature seem consistent with the usual Klemens–Callaway formalism, although detailed calculations are required to confirm this assertion.

Assuming a single mechanism is acting similarly on both properties the following picture is suggested. Consider currents between two particles in a sintered body as flowing essentially unimpeded where the particles are well fused to each other and not at all where the particles are not well fused, regardless of the reason for the lack of fusion. Estimation of the effective conductivities (thermal or electrical) of the body reduces to the topological problem of calculating the effective pathlength of the tortuously connected medium. In such a case both electrical and thermal current flow would be similarly affected, except at very high temperatures where radiation can contribute to heat transport.

If such defects are responsible for the observed reductions in k and σ, then little improvement the figure of merit of hot-pressed alloys as currently fabricated and other approaches must be used. The optimum doping level estimated from the data in Fig. 6 offers some modest room for growth. The optimum electrical power factors ($S^2\sigma$) for n- and p-type sintered $Si_{0.8}Ge_{0.2}$ are 3.93×10^{-3} and 2.31×10^{-3}W/m K^2, which occur at $S = -171\times\mu$V/K, $\sigma = 135\,000\ \Omega^{-1}\,m^{-1}$ and $S = 168\ \mu$V/K, $\sigma = 82\,000\ \Omega^{-1}\,m^{-1}$, respectively, as given by the theoretical fit at 1200 K. These values are close to those predicted for zone-leveled materials. Achieving the optimum carrier concentration may require doping beyond the solubility limit, particularly in n-type materials, possibly limiting the practical value of optimally doped materials. Due to the logarithmic dependence of S on σ, however, even a factor- of-2 deviation from optimum doping results in only about a 10% loss in electrical power factor.

V. SUMMARY AND CONCLUSIONS

The empirical values $ZT = 1$ previously found in zone-leveled $Si_{0.7}Ge_{0.3}$ has been achieved, but not significantly surpassed, in this study on sintered $Si_{0.8}Ge_{0.2}$. In spite of reductions in the thermal conductivity approaching 50% in fine-particle-size material, higher ZT values have not resulted due to associated reductions in electrical conductivity.

The apparent failure of phonon grain- boundary scattering theory to account for the qualitative temperature dependence of the thermal conductivity prompts the suggestion that transport in sintered silicon germanium differs from zone-leveled materials primarily due to the tortuous connectivity of the former compared to the latter. This suggestion also seems consistent with the observed effects of processing and the correlated nature of the variations in electrical and thermal conductivities. Finally, analysis indicates either acoustic or optical phonon scattering of the charge carriers dominates the temperature dependence of the high-temperature electrical properties.

ACKNOWLEDGMENTS

The authors wish to thank Dr. G. Slack, Dr. F. Rosi, Dr. J. Dismukes, and Dr. B. Abeles for useful discussions; S. Miller for preparing gas atomized powders; and S. Prochazka for performing the attrition milling. This work has been supported under U. S. Department of Energy contract No. DE-AC01-84NE32123.

[1] J. P. Dismukes, L. Ekstrom, E. F. Steigmeier, I. Kudman, and D. S. Beers, J. Appl. Phys. **10**, 2899 (1964).
[2] H. R. Meddins and J. E. Parrott, J. Phys. C **9**, 1263 (1976).
[3] D. M. Rowe, V. S. Shukla, and N. Savvides, Nature **290**, 765 (1981).
[4] D. M. Rowe and V. S. Shukla, J. Appl. Phys. **52**, 7421 (1981).
[5] C. M. Bhandari and D. M. Rowe, Contemp. Phys. **21**, 219 (1980).
[6] H. J. Goldsmid and A. W. Penn, Phys. Lett. **27A**, 523 (1968).
[7] J. E. Parrott, J. Phys. C **2**, 147 (1969).
[8] D. M. Rowe, J. Phys. D **7**, 1843 (1974).
[9] C. M. Bhandari and D. M. Rowe, J. Phys. D **10**, L10 (1977).
[10] C. M. Bhandari and D. M. Rowe, J. Phys. C **11**, 1787 (1978).
[11] N. Savvides and J. J. Goldsmid, J. Phys. C **13**, 4671 (1980).
[12] C. M. Bhandari and D. M. Rowe, in *Proceeding s of the Second International Conference on Thermoelectric Energy Conversion*, edited by K. R. Rao (IEEE, New York, 1978), p. 32.
[13] D. M. Rowe and R. W. Bunce, J. Phys. D **2**, 1497 (1969).
[14] N. Savvides and H. J. Goldsmid, J. Mater. Sci. **15**, 594 (1980).
[15] D. M. Rowe and C. M. Bhandarl, *Modern Thermoelectrics* (Reston, Reston, VA, 1983).
[16] P. G. Klemens, Proc. Phys. Soc. A **68**, 1113 (1955).
[17] J. Callaway, Phys. Rev. **113**, 1046 (1959).
[18] R. W. Bunce and D. M. Rowe, Mater. Sci. Eng. **2**, 278 (1967).
[19] P. R. Sahm and L. H. Gnau, Z. Metallkde. **59**, 137 (1968).
[20] D. M. Rowe, J. Phys. D **4**, 1816 (1971).
[21] R. D. Nasby and E. L. Burgess, in *Proceedings of the 7th Intersociety Energy Conversion Engineer Conference* (IEEE, New York, 1972), p. 130.
[22] R. K. Pisharody and L. P. Garvey, in *Proceedings of 13th Intersociety Energy Conversion Engineer Conference* (IEEE , New York, 1978), p. 1963.
[23] S. A. Miller, in *Amorphous Metallic Alloys*, edited by F. E. Luborsky (Butterworth, London, 1983).
[24] D. H. Stutz, S. Prochazka, and J. Lorenz, J. Am. Ceram. Soc. **68**, 479 (1985).
[25] K. Owusu-Sekyere, W. A. Jesser, and F. D. Rosi, Mater. Sci. Eng. B**3**, 231 (1989).
[26] L. J. van der Pauw, Philips Res. Rep. **13**, 1 (1958).
[27] R. E. Taylor and K. D. Maglic, in *Compendium of Thermophysical Property Measurement Methods*, Vol. 1, edited by K. D. Maglic, A. Cezairliyan, and V. E. Peletsky (Plenum, New York, 1984), p. 305.
[28] T. Amano, B. J. Beaudry, K. A. Gshneidner, Jr., R. Hartman, C. B. Vining, and C. Alexander, J. Appl. Phys. **62**, 819 (1987).
[29] N. Cusack and P. Kendall, Proc. Phys. Soc. London **72**, 898 (1958).
[30] G. H. Jonker, Philips Res. Rep. **23**, 131 (1958).
[31] B. R. Pamplin, in *Handbook of Chemistry and Physics*, 54th ed., edited by R. C. Weast (CRC, Cleveland, OH, 1973), p. E98.
[32] F. J. Morin and J. P. Maita, Phys. Rev. **96**, 28 (1954).
[33] C. H. Seager, Ann. Rev. Mater. Sci. **15**, 271 (1985).